Equilibrium Length and Shape of Rodlike Polyelectrolyte Micelles in Dilute Aqueous Solutions

Anja Kroeger,[†] Valadoula Deimede,[†,§] Joerg Belack,[†] Ingo Lieberwirth,[†] George Fytas,[†,‡] and Gerhard Wegner*,[†]

Max Planck Institute for Polymer Research, Ackermannweg 10, 55128 Mainz, Germany, and Department of Materials Science and Technology, University of Crete and F.O.R.T.H., P.O. Box 1527, 71110 Heraklion, Greece

Received August 25, 2006; Revised Manuscript Received October 31, 2006

ABSTRACT: Supramolecular structure formation in dilute salt-free aqueous solutions of highly charged dodecyl-substituted poly(*p*-phenylene)sulfonates (PPPS) in the free acid form (PPPS-H) with molar masses between $M_{w,p} = 21 \times 10^3$ and $M_{w,p} = 58 \times 10^3$ g/mol is investigated by static, isotropic, and anisotropic dynamic light scattering as well as transmission electron microscopy. The PPPS-H moieties, which are models of rodlike polyelectrolytes, form cylindrical micelles in which the shape of the formed objects can be analyzed in terms of a weakly bending rod by Koyama's form factor. The cylindrical micelles exhibit constant diameters ($d \sim 5$ nm) as well as radial and axial aggregation numbers ($N_{rad} \sim 15$ and $N_{ax} \sim 5$) but variable weight-average length depending on the polymer molar mass. The lengthwise aggregation is not controlled by kinetics. The inferred structures are supported by images obtained by transmission electron microscopy. TEM using different preparation methods reveals worm- and looplike micelles. Depending on the preparation conditions, the examined structures exhibit slightly different average diameters ranging from $d = 4.8$ to 8.0 nm. The occurrence of the various morphologies and their relevance for a mechanism by which equilibrium sized micelles can be obtained could be illustrated by means of a model based on the nematic character of the individual micelles. Besides the expected polyelectrolyte micelles, ternary superstructures, formed by association of several individual micelles, were found.

Introduction

Conformationally rigid and rodlike polyelectrolytes represent ideal model systems because they have a shape-persistent backbone; thus, their conformation is independent of the ionic strength in the system.[1] In the case of flexible polyelectrolytes, a decrease of the ionic strength may lead to an expansion of the coils due to strong intramolecular forces as well as to stronger intermolecular electrostatic interactions.[2−4] Stiff-chain polyelectrolytes, on the other hand, remain in their extended chain conformation. Consequently, only intermolecular Coulombic interactions, and at higher concentration excluded volume forces determine the solution properties of these polymers.[5]

On the basis of these considerations, Rulkens et al.[6] and Bockstaller et al.[7] have introduced a simplified synthetic model system for systematical investigations, namely poly(*p*-phenylene)sulfonate (PPPS). As shown in Figure 1 the primary structure of this model polymer consists of a poly(*p*-phenylene) backbone with a persistence length $l_p = 12.6$ nm.[8] Every third phenylene ring is substituted with one methyl and one dodecyl side group. The two remaining phenylene rings per repeat unit carry each just one sulfonic acid residue. This substitution scheme generates a hydrophilic and a hydrophobic part of the macromolecule. The embedded hydrophobic-hydrophilic balance results in the strong tendency of PPPS to form a well-defined secondary structure. Previous works[9,10] have shown that this secondary structure in water can be described as highly anisotropic cylindrical micelles of a number of poly(*p*-phenylene) chains

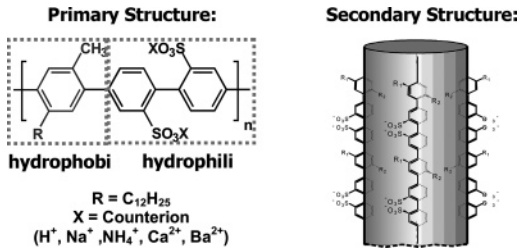

Figure 1. Primary structure of the alkyl-substituted sulfonated poly(*p*-phenylene) and a schematic picture of a section of a single cylindrical micelle (secondary structure). The hydrophobic and hydrophilic parts of the chemical repeat unit of the polymer are indicated in the primary structure.

oriented parallel to the cylinder axis characterized by the radial aggregation number N_{rad} at which chain end pairing in nematic packing occurs to reduce the strain created by individual chain ends. Within these aggregates the hydrophobic aliphatic side chains are oriented inward and the ionic groups are located at the outer surface of the cylindrical structure. The micelles have a contour length much larger than the length of the constituent macromolecules characterized by an axial aggregation number N_{ax}. The formed micelles of PPPS in water are rather stable objects, which undergo further interactions to form tertiary and even quaternary structures.[10,11] Even at the lowest examined concentration ($c_p \sim 8 \times 10^{-4}$ g/L), at which scattering experiments can be conducted, only micelles were identified and hence the critical micelle concentration is immeasurably small. Studies by Bockstaller et al.[10,12] on the sodium salt form of PPPS (PPPS−Na) and more recently[15] on the free acid form (PPPS-H) in water revealed single cylindrical objects forming an isotropic solution up to a critical concentration of $c_{crit.} \sim 0.02$ g/L at 20 °C. This value is slightly influenced by the molar mass of the constitutive polymer, the counterion species and

* Corresponding author. E-mail: wegner@mpip-mainz.mpg.de.
[†] Max Planck Institute for Polymer Research.
[‡] Department of Materials Science and Technology, University of Crete and F.O.R.T.H..
[§] Present address: ICEHT-F.O.R.T.H., Patros, Greece.

10.1021/ma061966j CCC: $37.00
Published on Web 12/14/2006

Table 1. Sample Specification

sample	PPPS-H21	PPPS-H30	PPPS-H42	PPPS-H58
$M_{w,p}$ (10^3 g/mol)	21 ± 2	30 ± 3	42 ± 4	58 ± 6
$L_{W,p}$ (nm)	25 ± 3	36 ± 4	50 ± 5	70 ± 7
dn/dc (mL/g)	0.189 ± 0.02	0.181 ± 0.02	0.181 ± 0.02	0.222 ± 0.02

the temperature. Above $c_{crit.}$, the micellar objects start to associate into aggregates composed of a small number of micelles at a defined concentration and these aggregates give rise to a gel phase at still higher concentration. Rulkens et al.[9] as well as Zaroslov et al.[13] have reported that under certain conditions of experimental parameters lyotropic liquid crystal phases of the micelles could be identified. However, the aggregation behavior and nature of the lyotropic phase seems to depend on the chain length of the primary macromolecules, the counterion species, and ionic strength of the solution.[14]

In a previous study, we have reported about the influence of counterion on the aggregation behavior.[15] The aim of the present paper is, therefore, to elucidate the role of the molar mass of the polymer on the self-organization of these wormlike polyelectrolytes by using various light scattering techniques. While light-,[9,10] X-ray-,[9] and neutron-scattering[13] data help one to assess the integral structure of the micelles and their aggregation behavior, the data evaluation needs a model of the structure of the individual objects and their interaction. Here, direct imaging methods come in to play which help to corroborate the assumptions which enter the interpretation of the scattering data. Moreover, details which are difficult or even impossible to retrieve from scattering data can be observed in direct space of appropriate imaging methods. In the present work the morphology of PPPS-H was investigated by applying the imaging technique via transmission electron microscopy (TEM). A combined and critical discussion of the pertinent results of structure elucidation by direct imaging as well as by scattering experiments allows identifying the "true" nature of these supramolecular structures as well as mechanisms behind their formation and interactions.

Experimental Section

Materials. Details of the synthesis of PPPS have been reported elsewhere.[16,17] In this work five different samples of the free acid form (PPPS-H), PPPS-H21, -H30, -H42, -H54, and -H58, with weight-average molar masses of the polymers between $M_{w,p} = 21$ kg/mol and $M_{w,p} = 58$ kg/mol and similar polydispersity $M_{w,p}/M_{n,p} \approx 2$ were studied under salt-free conditions. In other words, only hydrated protons serve as counterions in water as the solvent. The purity of the samples was controlled by atomic absorption spectroscopy (AAS), because previous studies[15] had shown that very small amounts of ionic impurities have a strong effect on the structure formation.

Photon Correlation Spectroscopy (PCS). Dilute aqueous solutions of PPPS-H with a concentration of $c_p = 3.4 \times 10^{-3}$ g/L were prepared by dilution of a stock solution of $c_p = 0.34$ g/L, which was made by dissolving the samples in ultrapure Milli-Q water of a conductivity <18.2 MΩ·cm under continuous stirring for several hours. Subsequently, for light scattering experiments dust-free solutions were obtained by filtration through cellulose acetate membrane filters with a pore size of 0.45 μm (Millipore, Millex-HA) into cylindrical silica glass cuvettes (Hellma, inner diameter, i.d. = 20 mm), which had been cleaned before with acetone in a Thurmont apparatus.[18] The concentration in the aqueous solution after filtration was also verified by UV-spectroscopy. The required refractive index increment dn/dc for each sample of PPPS-H was measured at $\lambda = 633$ nm using a scanning Michelson interferometer.[19] The dn/dc values are listed in Table 1.

Light scattering measurements were performed on a commercially available ALV spectrometer consisting of a goniometer and an ALV-5000 full digital correlator (320 channels) which allows dynamic light scattering measurements over a time range $10^{-7} \leq t \leq 10^3$ s. A Kr-ion laser (Spectra Physics model 2020 with a single mode intensity of 100 mW operating at $\lambda_0 = 647.1$ nm), and a Nd:YAG dye-pumped, air-cooled laser (Adlas DPY 325 with a single mode intensity of about 50 mW operating at $\lambda_0 = 532$ nm) were used as light sources. All measurements were carried out at temperature $T = 20$ °C. For all light scattering experiments, Glan-Thomson polarizers with an extinction coefficient better than 10^{-7} were used which allows detecting a change of the polarization of the scattered light. Here, the first polarizer guarantees that only vertically (V) polarized light meets the sample and the second polarizer, the analyzer, may be redirected from the vertical (VV) to the horizontal (VH) position with respect to the scattering plane for depolarized dynamic experiments.

Static light scattering experiments (SLS) were performed over an angular range from 12° to 150° corresponding to a scattering vector q in a range of $3.29 \times 10^{-3} < q < 3.04 \times 10^{-2}$ nm^{-1} with $q = (4\pi n_{solv}/\lambda_0) \sin(\theta/2)$ where n_{solv} is the refractive index of the solvent (for water $n_{solv} = 1.33$), θ denotes the scattering angle and λ_0 is the wavelength of the incident laser beam. The reduced absolute intensity ratio $R(q)/(Kc)$ at a concentration c, is computed from the Rayleigh ratio $R(q)$,

$$R(q) = \frac{I(q)_{soln} - I(q)_{solv}}{I(q)_t}\left(\frac{n_{solv}}{n_t}\right)^2 R_t \qquad (1)$$

and the optical constant $K = (2\pi n\ \mathrm{d}n/\mathrm{d}c)^2/(\lambda_0^4 N_A)$; I_{soln}, I_{solv}, and I_t are respectively the light scattering intensities of the solution, solvent, and the pure toluene which is used as a standard with refractive index $n_t = 1.496$ and Rayleigh ratio $R_t = 2.78 \times 10^{-5}$ cm^{-1} at $\lambda_0 = 532$ nm and $R_t = 9.52 \times 10^{-6}$ cm^{-1} at $\lambda_0 = 647.1$ nm whereas N_A is the Avogadro number.[20]

In dynamic light scattering (DLS), the experimental normalized autocorrelation function $G(q, t) = \langle I(q,0)I(q,t)\rangle/\langle I(q)\rangle^2$ of the light scattering intensity $I(q)$ at q is related to the normalized time correlation function $g(q,t) = \langle E^*(q,0)E(q,t)\rangle/\langle|E(q,0)|^2\rangle$ of the scattered electric field $E(q,t)$ by the Siegert relation

$$G(q, t) = 1 + f^*|\alpha g(q, t)|^2 = 1 + f^*|C(q, t)|^2 \qquad (2)$$

where f^* is a coherence instrumental factor and α denotes the fraction of the total scattered intensity $I(q)$ associated with fluctuations relaxing with times longer than 0.1 μs.[21] To analyze the computed relaxation functions $C(q,t)$, an inverse Laplace transformation using the constraint regularized CONTIN method was applied.[22] This method assumes that $C(q,t)$ can be represented by a superposition of exponentials,

$$C(q, t) = \int_{-\infty}^{\infty} H_\tau(\ln \tau)\, \exp[-t/\tau]\, d(\ln \tau) \qquad (3)$$

where $H_\tau(\ln \tau)$ is the distribution of relaxation times. The characteristic relaxation times correspond to the peak positions of $H_\tau(\ln \tau)$ and the area under the peak defines the value α (eq 2) and hence the intensity $\alpha I(q)$ associated with the particular dynamic process. For single but nonexponential decay, $C(q,t)$ can be represented by the stretched exponential Kohlrausch−Williams−Watts (KWW) function

$$C(q, t) = \alpha \exp[-(t/\tau^*(q))^\beta] \qquad (4)$$

where the shape parameter $0 < \beta \leq 1$ characterizes the distribution of relaxation times.[23]

Transmission Electron Microscopy (TEM). Specimens were studied using either a Zeiss EM 902 or a Philips CM12 transmission

electron microscope operated at 80 or 120 kV respectively. Electron micrographs were recorded on Ilford PanF film.

(a) Samples Adsorbed on a Carbon Support Film. A drop of the dilute aqueous polymer solution of PPPS-H54 prepared as described above ($c_p \sim 2 \times 10^{-3}$ g/L) was deposited directly onto a thin carbon support film mounted on a 300 mesh copper EM grid held by a pair of fine forceps. Most of the water was removed by touching the grid edge to a filter paper wedge, and the sample was allowed to dry in the open under room conditions.

In order to increase the contrast of the sample in the TEM additional staining was employed. The single droplet procedure[24] was used with consecutive application of polymer solution ((0.1−2) × 10^{-3} g/L) and negative stain (1−5% w/v aqueous uranyl acetate or 1−5% w/v aqueous ammonium molybdate) to carbon support films on 300 mesh copper EM grids. After careful removal of excess sample and stain by touching the grid edge to the edge of a filter paper wedge, the samples were allowed to air-dry at room temperature.

In some cases, staining of the samples was realized using the "washing" procedure: first the sample solution was applied to the carbon-coated EM grid and most of the solution was removed by blotting with the edge of a filter paper. Afterward, the staining solution was applied three to four times in the same way before the sample was finally dried as the other samples.

For the freeze drying procedure, a drop of the aqueous sample solution ($c_p = 2 \times 10^{-3}$ to 2×10^{-4} g/L) was pipetted directly to a carbon grid and blotted with filter paper to create a thin layer of the sample solution on the grid surface. The grid was rapidly plunged into liquid ethane (using a free-fall rapid plunge-freezing apparatus) producing a thin layer of vitreous water. Subsequently, all the vitrified water was removed via sublimation at −88 °C in vacuum ($p \sim 2 \times 10^{-5}$ mbar). Careful attention was paid to keep the sample well below −90 °C while transferring it from the plunging machine to the precooled vacuum vessel.

(b) Sample Preparation without Support Film. In order to avoid interaction of the polymer in its various forms of aggregation with any support surface the sample was embedded in a self-supporting electron transparent thin film of trehalose following the method of Harris.[24,25]

Sample droplets ($c_p = 2 \times 10^{-3}$ g/L) were applied to a holey carbon support film mounted on an EM grid and some of the fluid was removed by touching the grid to the edge of a filter paper wedge. Then trehalose solution (0.1−1% w/v) was applied in the same manner. At the final stage, maximal removal of the sample−trehalose mixture was necessary (again by blotting it off by filter paper) in order to obtain a thin film of the trehalose matrix with the sample embedded spanning the holes of the template support film after the sample has been allowed to dry at ordinary conditions. Imaging these samples in the TEM the contrast is very low because the difference in electron density between the embedded polymer structures and the surrounding matrix is rather low. Thus, additional negative staining was applied by adding either 5% w/v uranyl acetate or ammonium molybdate to the trehalose solution.

In order to enlarge the field of inspection on the sample (the holes) 600 mesh hexagonal copper EM grids have been used sometimes instead of the holey carbon templates.

Results and Discussion

I. Light Scattering. SLS. Static light scattering experiments in very dilute solutions gives information about shape, size and molar mass of the single investigated species. In aqueous solutions of PPPS, single polymer molecules cannot be detected even at a concentration as low as $c_p = 8 \times 10^{-4}$ g/L. Instead, the polyelectrolyte exists in the form of supramolecular objects which are micelles with dimensions of the order of few hundred nanometers as recorded earlier.[10,15] However, in very dilute solutions an extensive structural characterization of individual assemblies is possible, because intermolecular interactions between the micelles should not play a significant role. Hence, for this study very dilute solutions with a polymer concentration of $c_p = 3.4 \times 10^{-3}$ g/L were always used.

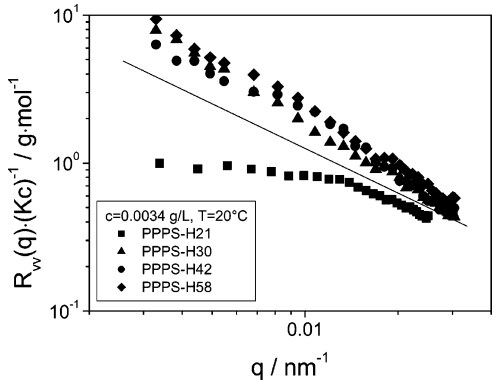

Figure 2. Absolute static light scattering intensity for several PPPS-H samples at $c_p = 3.4 \times 10^{-3}$ g/L as a function of q. The line denotes a slope of $R_{VV}(q) \propto q^{-1}$, which is expected for rodlike objects.

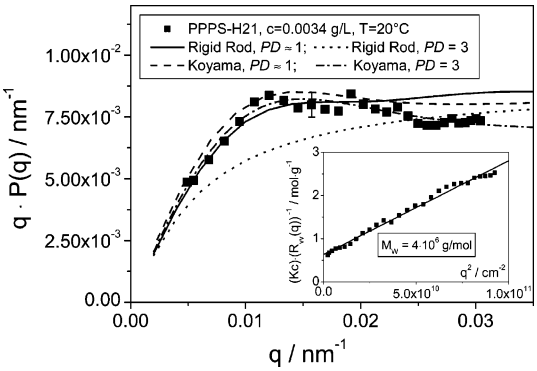

Figure 3. Holtzer plot of the static light scattering intensity of PPPS-H21 in salt-free solution at $c_p = 3.4 \times 10^{-3}$ g/L. The lines denote different form factors. The inset shows the plot of $Kc/R_{VV}(q)$ vs q^2 for the determination of the molar mass and the radius of gyration of the micellar structure.

The angular dependence of the measured total scattered intensity which is presented as $R_{VV}(q)/(Kc)$ vs q is shown for several samples in Figure 2. The measured q dependence of $R_{VV}(q) \propto q^{-1}$ as illustrated in Figure 2 by a solid line is typical for rodlike objects. At low q values the scattered intensity of PPPS-H21 approaches the Guinier regime. With increasing $M_{w,p}$ an increasing total scattered intensity is observed, which indicates a molecular weight dependence of the formed assemblies. The determination of the shape and dimension of the structures are the first targets. Therefore, Figure 3 shows a Holtzer presentation of the form factor $P(q) = R_{VV}(q)/(M_w/Kc)$ of PPPS-H21 as a function of the scattering vector q. The weight-average molar mass M_w of the supramolecular assembly is obtained from the $Kc/R_{VV}(q)$ vs q^2 plot in the linear regime at low q values as shown in the inset of Figure 3. The intercept and the slope of this Ornstein−Zernicke plot respectively yields $M_w = (4 \pm 0.5) \times 10^6$ g/mol and of the radius of gyration $R_G = (144 \pm 9)$ nm, as listed in Table 2. On the basis of the form of the experimental $qP(q)$, which increases at low q values and reaches a horizontal asymptote in the high q range, we conclude that the overall size of the micelles are probed. Thus, the experimental conditions justify the unambiguous determination of M_w and the estimation of the overall size $2p/q_m \sim 500$ nm from the value of q_m at which $qP(q)$ exhibits its maximum. In Figure 3, the experimental data are represented by the symbols, whereas the lines describe various theoretical form factors. At

Table 2. Characteristics of the Self-Assembled Structures in Aqueous Salt-Free Solutions at $c_p = 3.4 \times 10^{-3}$ g/L and $T = 20$ °C Obtained by SLS

sample	M_w (10^6 g/mol)	L_W (nm)	N_{rad}	N_{ax}	R_G (nm)	M/L (10^3 (g/mol) nm^{-1})
PPPS-H21	4.0 ± 0.4	560 ± 30	14 ± 3	5 ± 1	144 ± 9	7.2 ± 0.8
PPPS-H30	5.5 ± 0.6	630 ± 40	17 ± 3	4 ± 1	160 ± 10	8.8 ± 1.0
PPPS-H42	10.5 ± 1.1	1170 ± 60	18 ± 4	5 ± 1	190 ± 12	9.4 ± 1.0
PPPS-H58	12.8 ± 1.3	1600 ± 80	16 ± 3	5 ± 1	281 ± 18	8.0 ± 0.9

first we assumed a rigid rod shape of the objects. The well-known formula for the angular distribution of scattered light by a system of monodisperse rods of length L and a negligible diameter given by[26]

$$P_{rod}(q) = \frac{2}{qL}\left[\int_0^{qL} \frac{\sin u}{u}\,du\right] - \left(\frac{\sin qL/2}{qL/2}\right)^2 \quad (5)$$

leads to the solid line in Figure 3. However, this theoretical $P(q)$ does not describe the experimental $P(q)$ sufficiently, well mainly in the peak region as well as at high q values. Because the samples are not monodisperse, the formed aggregates should be exhibit a size polydispersity. The size polydispersity PD as inferred from the nonexponential shape of the relaxation function for the concentration and orientation fluctuations (see below) has to be considered in the computation of the appropriate form factor $P(q)$

$$P_z(q, L, W) = \frac{\int_0^\infty P(q)W(L)L\,dL}{\int_0^\infty W(L)L\,dL} \quad (6)$$

where $W(L)$ denotes the distribution of contour lengths L assuming to be of a Schulz-Zimm type

$$W(L) = \frac{L^m}{m!}y^{m+1}e^{-yL} \quad (7)$$

with $y = (m + 1)/L_W$, where m is a parameter characterizing the polydispersity of the structures $[m^{-1} = (L_W/L_{n-1})]$.[27] The introduction of $PD = 3$ according to eq 6 and ep. 7 into eq 5 worsens the fit significantly, as shown by the dotted line in Figure 3. Thus, the cylindrical micelles which possess semiflexibility approach the rigid rod limit due to relatively high contour length. For weakly bending rods, an alternative approximate solution was proposed by Koyama[15,28]

$$P_{Koyama}(L_r, ql_k) = \frac{2}{L_r^2}\int_0^{L_r}(L_r - x)\exp\left[-\frac{1}{3}s^2 x f(x)\right]\frac{\sin(s\,x g(x))}{s\,x g(x)}dx \quad (8)$$

with L_r being the reduced contour length $L_r = 2\mu L$, μ the inverse of l_k the Kuhn segment length of the scattered structure, $s = (q/2\mu)$ denotes the reduced q and x is the number of segments per reduced length. Besides the Koyama method similar form factor analyses are possible on the basis of Schurtenberg/Pederson and Kholodenko as described in ref 28d. We employ this form factor to represent the experimental $P(q)$ mainly because of the resemblance of the present structures more to rod rather than to coil conformations. The dashed line in Figure 3 denotes the Koyama form factor according to eq 8 for monodisperse structures with $L = 600$ nm, and a Kuhn segment length $l_k = 350$ nm which capture the experimental R_G. The computed $P(q)$ displays deviations from the experimental data at high q values. Inclusion of size polydispersity (eq 6 and 7) into the Koyama form factor (eq 8) with $PD = 3$ clearly leads to a better representation of the experiment as shown by the dash dotted line in Figure 3. This form factor analysis can be employed for all samples. Thus, Figure 4 gives a Holtzer presentation of the form factors $P(q)$ of the samples PPPS-H21, -H42, and -H58 as a function of q. The symbols correspond invariably to the experimental data and the solid lines describe the corresponding Koyama form factors (eq 8) respectively with $PD = 3$. The increasing dimension of the formed micelles as indicated in Figure 2, are characterized by an increasing scattered intensity $I(q)$ as well as a shift of the peak maxima of $qP(q)$ against lower q values. This effect has to be interpreted in terms of in the Koyama form factor as due to a rise in the Kuhn segment number $N_k = L/l_k$, because l_k remains constant as a result of the conformational rigidness of PPPS. According to this a theoretical adaptation of Koyama's $P(q)$ results for PPPS-H42 in $L = 1700$ nm and $L = 2300$ nm for PPPS-H58. Because of an increasing contour length of the formed objects an increasing inaccuracy of Koyama's model results which appears at high q values. The weight-average molar mass of this samples $M_w \sim (11-13) \times 10^6$ g/mol is obtained from the Ornstein−Zernicke plot as described above and listed in Table 2. The plateau values of the horizontal asymptote in the high q range allows to estimate the linear mass density

$$M/L = \frac{qR_{VV}(q)}{cK\pi} \quad (9)$$

and from M/L the weight-average length of the objects

$$L_W = \frac{M_w}{(M/L)} \quad (10)$$

are obtained. There is a good agreement between L determined by the form factor analysis and the contour length of the formed micellar objects L_W as estimated from the angular dependence of the static scattering intensity by eq 10 as summarized in Table 2.

Once M_w and L_W of the micelles are known, the radial aggregation number N_{rad} which is the average number of polymer chains per cross section of the cylindrical micelles, can be estimated by

$$N_{rad} = \frac{M_w}{L_W}\frac{L_m}{M_m} \quad (11)$$

with $M_m = 571$ g/mol and $L_m = 1.2$ nm being the molar mass and the length of the monomer unit. As shown in Table 2 for all samples $N_{rad} = 14-18$ are obtained, which are considered to be identical within the experimental error. Here, the limited variations likely base on fluctuations of the number of polymer chains per cross section along the cylindrical structures. It should be well understood that N_{rad} is an average value; however, large fluctuations do not seem to occur as is evident from the analysis of TEM micrographs to be discussed in section II.

It should be mentioned that PPPS−Na in water[10] and a short chain nonionic amphiphilic PPP in surfactant solution[29] also

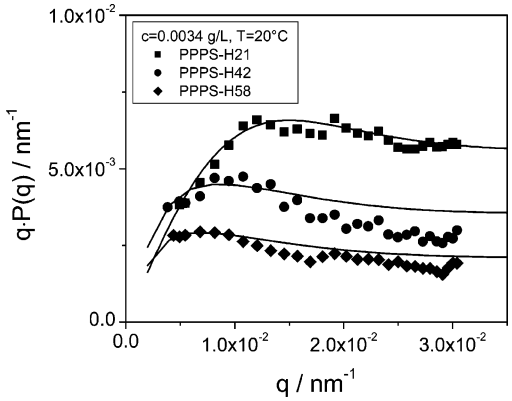

Figure 4. Holtzer plot of the static light scattering intensity of PPPS-21, -H42, and -H58 in salt-free solution at $c_p = 3.4 \times 10^{-3}$ g/L. The solid lines describe the corresponding Koyama form factor respectively with $PD = 3$.

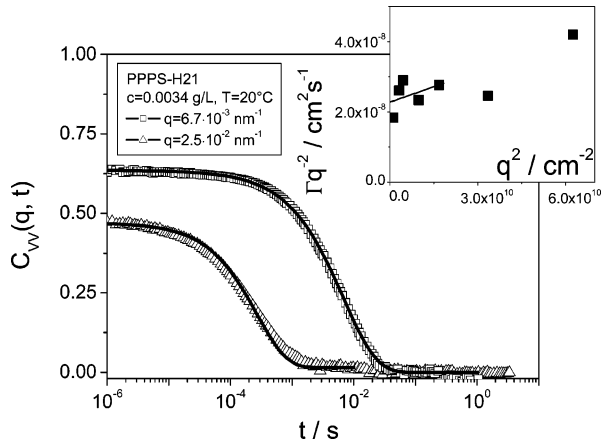

Figure 5. Relaxation functions $C(q,t)$ for the concentration fluctuations in 3.4×10^{-3} g/L PPPS-H21 for $q = 6.7 \times 10^{-3}$ nm^{-1} (□) and $q = 2.5 \times 10^{-2}$ nm^{-1} (Δ) at 20 °C. The solid lines denote representations according eq 12. The shape of the experimental $C(q,t)$ at high q is broader ($\beta = 0.71$) than the theoretical function ($\beta = 0.85$). The diffusion coefficient Γ/q^2 obtained from the experimental $C(q,t)$ is shown as a function of q^2 in the inset whereas the solid line denotes a linear dependence (eq 13).

form micelles with $N_{rad} \sim 15$. The radial aggregation number of these structures is determined by the packing density of the nonpolar dodecyl side groups, which fill the interior of the cylindrical micelles and do not depend on the molar mass of the polymers. Furthermore, Bockstaller et al.[10] have shown that the axial aggregation number $N_{ax} = L_n/L_m$ also remain constant. Our studies confirm these results. Thus, the axial aggregation number which described the number of constitutive chains along the cylinder axis assumes values of $N_{ax} \sim 5$ as listed in Table 2. Hence, N_{ax} is molar mass as well as counterion independent. It seems to be controlled by an intrinsic mechanism which gives an equilibrium length distribution of the cylindrical micelles.

A mechanism explaining how the equilibrium length of the micelles is established will be proposed in consequence of real space information obtained via TEM micrographs (cf. Figure 13).

DLS. For completion the structure analysis of the formed micellar aggregates of PPPS-H in water dynamic light scattering experiments can be preformed. Figure 5 displays the relaxation function $C(q,t)$ (eq 2) for the PPPS-H21 system at $q = 6.7 \times 10^{-3}$ nm^{-1} and $q = 2.5 \times 10^{-2}$ nm^{-1}. We first assume one single translational diffusion mechanism for the decay of the concentration fluctuations in the dilute solution of these polydisperse objects.[21]

$$C(q,L,t) = \frac{\int_0^\infty P(qL)LW(L)e^{-D_z q^2 t}\,dL}{\int_0^\infty LW(L)\,dL} \qquad (12)$$

At low q values, eq 12 adequately describes the experimental $C(q,t)$ as shown by the solid line in Figure 5. Because of the domination of the scattering at low q values by the large objects the moderate width of the $C(q,t)$ is also described by eq 4 with $\beta = 0.83$. At the highest q, eq 12 predicts (solid line in Figure 5) a narrower shape ($\beta = 0.85$) than found experimentally ($\beta = 0.71$). This disparity is observable for all samples, as summarized in Table 3. It is attributed to an additional source of scattering due to internal degrees of freedom in the supramolecular assemblies. This additional contribution might affect the $I(q)$ in the high q range but there is no obvious way to account for it. For large particles, the reduced first cumulant, Γ/q^2, shows a q dependence that can be written in the low q range limit as[21,30]

$$D_{app}(q) = \frac{\Gamma}{q^2} = D_z[1 + C(R_G{}^2 q^2) - ...] \qquad (13)$$

where C is a dimensionless structure sensitive parameter depending on the molecular architecture and polydispersity of the particles.[21]

The translational diffusion coefficient $D_z = 2.3 \times 10^{-8}$ cm^2 s^{-1} obtained from the intercept of the linear variation of Γ/q^2 (see inset to Figure 5) with q^2 is also a conformation index of the diffusing objects. For rigid rods[31] of length L_z and diameter d

$$D_Z = \frac{k_B T}{3\pi\eta_0 L_Z}\left(0.58 + \ln\frac{L_Z}{d}\right) \qquad (14)$$

where η_0 is the solvent viscosity. Using $d = 5$ nm, the experimental D_z leads to $\langle 1/L\rangle_z^{-1} = 1000$ nm which encourages the found size polydispersity of $PD = 3$. For semiflexible chains with Kuhn segments length l_k, an alternative expression[20,32] can be also applied assuming a value for L_z as obtained from the static form factor $P(q)$ (Figure 3 and 4). In this case, l_k takes a value between 400 nm and L_z that again supports a rigid structure.

DDLS. The presence of large optical anisotropic objects in very dilute solution can be studied by depolarized dynamic light scattering and yields in information about the rotational dynamics and internal structures. Admittedly, this information is often lost due to a too weak intensity signal and a too strong signal-to-noise ratio. Therefore, the horizontal part of the scattered light of sample PPPS-H21 cannot evaluated, only the measured intensity is obtained. For the other samples orientation relaxation functions $C_{VH}(q,t)$ are determinable in the q range $3.29 \times 10^{-3} < q < 6.81 \times 10^{-3}$ nm^{-1}. Figure 6 represents the normalized autocorrelation functions (eq 2) for concentration $C_{VV}(q,t)$ and orientation fluctuations $C_{VH}(q,t)$ of PPPS-H58 at $q = 4.11 \times 10^{-3}$ nm^{-1}. The relaxation function for orientation fluctuations $C_{VH}(q,t)$ decays via both translational and rotational motion, and hence for polydisperse rigid rods[31]

$$C_{VH}(q,t) = \frac{\int_0^\infty LW(L)\exp[-(D_z q^2 + 6D_R)t]\,dL}{\int_0^\infty LW(L)\,dL} \qquad (15)$$

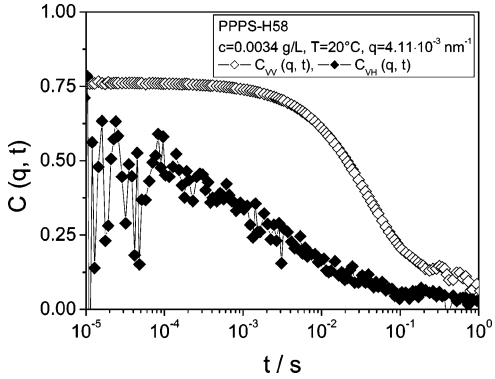

Figure 6. Relaxation function $C_{VV}(q,t)$ and orientation relaxation function $C_{VH}(q,t)$ at $q = 4.11 \times 10^{-3}$ nm^{-1} for an aqueous solution of PPPS-H58 with $c_p = 3.4 \times 10^{-3}$ g/L at 20 °C.

Table 3. Characteristics of the Self-assembled Structures in Aqueous Salt-Free Solutions at $c_p = 3.4 \times 10^{-3}$ g/L and $T = 20$ °C Obtained by DLS

sample	D_z (10^{-8} cm^2 s^{-1})	R_h (nm)	β at $q = 8.15 \times 10^{-3}$ nm^{-1}	β at $q = 3.04 \times 10^{-2}$ nm^{-1}
PPPS-H21	2.3 ± 0.2	93 ± 9	0.83	0.71
PPPS-H30	1.3 ± 0.1	165 ± 17	0.87	0.75
PPPS-H42	1.3 ± 0.1	165 ± 17	0.83	0.73
PPPS-H58	1.7 ± 0.2	126 ± 13	0.89	0.59

Table 4. Characteristics of the Self-Assembled Structures in Aqueous Salt-Free Solutions at $c_p = 3.4 \times 10^{-3}$ g/L and $T = 20$ °C Obtained by DDLS

sample	D_R (s^{-1})	Γ_{VH} (s^{-1})	$L_{W\ VH}$ (nm)	$\langle\gamma^2\rangle/M_w$ (mol g^{-1})
PPPS-H21				$56-88\beta_t^2$
PPPS-H30	47 ± 5	280 ± 30	750 ± 75	$77\beta_t^2$
PPPS-H42	48 ± 5	286 ± 30	750 ± 75	$83\beta_t^2$
PPPS-H58	12 ± 2	69 ± 10	1230 ± 120	$60\beta_t^2$

where the relaxation rate $\Gamma_{VH}(q) = D_z q^2 + 6D_R$ yields the rotational diffusion

$$D_R = \frac{3k_BT}{\pi\eta_0 L^3}\ln\left(\frac{L}{d}\right) \tag{16}$$

which allows an estimation of the contour length $L_{W\ VH}$ by using a micelle diameter of $d = 5$ nm.[15] A comparison of $L_{W\ VH}$ as listed in Table 4 and L_W as shown in Table 2 results in a good agreement of the values in consideration of the experimental error. This fact is an additional evidence for the predominate rodlike structure of the scattered objects and so all light scattering techniques ($P(q)$, D_z, and D_r) are compatible with rodlike micellar structures in aqueous solutions.

The q dependence of the amplitude $I_{VH}(q,L)$ in eq 15 is determined by the orientation correlations within the object with optical anisotropy $\langle\gamma^2\rangle = \beta_t^2(I_{VH}(q = 0)/c)/(I_{VH,t}/\rho_t)(M_t/M_w)$ where the quantities with subscript t refer to the standard toluene with optical anisotropy β_t^2, molar mass M_t and density ρ_t. The effective optical anisotropy $\langle\gamma^2\rangle/M_W$ yields in information about the degree of orientation of the phenyl rings of the constitutive polymer chains within the aggregates. As shown in Table 4 $\langle\gamma^2\rangle/M_w$ is independent of the molar mass of the polymer, because the orientation of the backbone phenyl rings are influenced by the ionic strength in the solution and this remains constant.

II. Transmission Electron Microscopy. Figure 7 presents a set of TEM images of air-dried PPPS-H54 samples negatively stained with 2% uranyl acetate adsorbed on a carbon-coated grid. Various morphologies such as worm- or threadlike

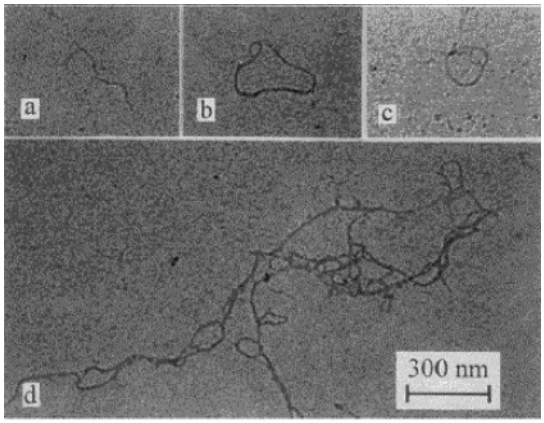

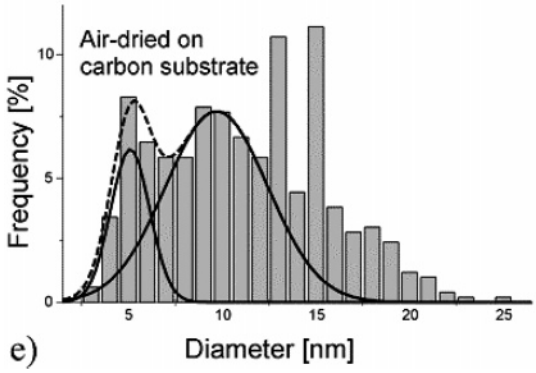

Figure 7. (a−d) TEM micrographs of air-dried PPPS-H54 supramolecular structure negatively stained with 2% uranyl acetate and deposited on a carbon-coated grid: (a) rodlike structures, (b) rodlike structures coexisting with others having loops at either end, (c) extended network consisting of micelles and loops, and (d) loop formed by winding around a preformed loop at one end of a wormlike structure. (e) Histogram showing the thickness distribution for the rodlike structures.

structures (Figure 7a) that sometimes coexist with loops at either end (Figure 7b) or looplike structures of threads (Figure 7c) were observed. The contour length of these objects exceeds several hundreds of nm and reaches several microns for the object depicted in Figure 7d. Note that the contour length of the constituent PPPS-H54 macromolecules is, on average, only ~100 nm ($L_{W,p} = 65$ nm). The average diameter of the represented structures amounts to 11.9, 11.8, and 12.6 nm for Figure 7, parts a, b, and c, respectively. These diameters correspond to independent data obtained by SFM.[33] Occasionally, extended networks consisting of interwoven wormlike threads which also form loops (Figure 7d) were also found. A histogram of diameters (Figure 7e) observed for the PPPS-H54 micelles prepared on a carbon substrate with addition of 2% uranyl acetate (Figure 7e) reveals a rather broad thickness distribution ranging from around 2 to 25 nm. In this histogram both, the network structures as well as the thread- and looplike structures are included. Remarkably, some populations are dominant. The first two maxima have been fitted by a Gaussian distribution function neglecting the data exceeding 12 nm diameter yielding mean values of $d = 5.1$ and 9.7 nm. The further two peaks found at higher values have not been fitted because their appearance strongly depends on the parameters chosen for the representation of the histogram. Nonetheless, attributed to these data, there is strong evidence for preferred diameters at higher values. This interpretation of the data takes the following into account: (a) the micelles interact with the surface of the carbon support film and thus may suffer from structural deformation and flattening and (b) the polymer

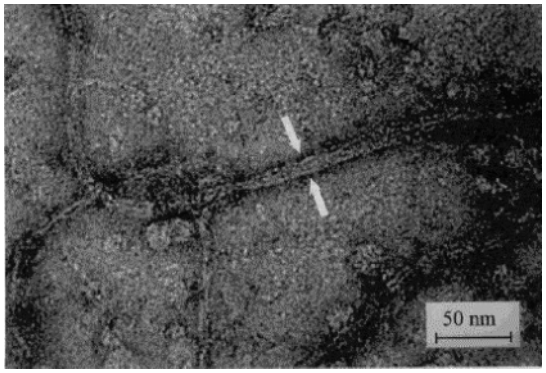

Figure 8. TEM micrograph of PPPS-H54 micelles adsorbed on a carbon surface. The sample was prepared be staining with uranyl acetate using the excess washing method.

concentration increases locally during the drying process. The latter will consequently lead to a situation described in the phase diagram for higher concentrations, that is the formation of bundles (clusters) and networks of micelles. The observed multiplicity of populations in diameter (Figure 7e) points into the direction that during the drying process single micellar structures assemble, forming parallel superstructures consisting of two, three, or more individual micelles. This point of view is substantiated by observation: as an example, Figure 8 shows the alignment of three individual micelles in a section of a threadlike superstructure. This sample was prepared on a carbon support and stained using the washing method which leads to an excess of staining agent and thus gives a negative staining contrast. Marked by the arrows, one can observe a long rodlike superstructure of $d \sim 10$ nm which consists of three individual, parallel threads. The diameter of the individual substructures amounts to $\sim 2.5-3$ nm, and we assume that these are the micelles depicted in Figure 1.

The formation of such more complex assemblies is attributed to the increase in concentration during the drying process. Hence, in order to preserve the native structure of the original aggregation forms, that is the individual micelles, sample solutions were freeze-dried. The structures which in this way were captured in the vitrified film were thus observed without dehydration and were so quickly vitrified that reorganization is less likely to occur. The micrographs of the freeze-dried samples deposited on a carbon substrate are shown in Figure 9. In this case, similar structures as for the air-dried preparation (Figure 7) are observed except of micellar networks. These were not observed with this preparation method. Quantitative image analysis of a large number of PPPS-H superstructures prepared by freeze drying on a carbon substrate reveals a diameter distribution ranging from around 3 to 12 nm with the maximum located around $d = 6.8$ nm (Figure 9d). This value is about 30% larger than predicted from the SAXS, SANS and TEM experiments which come to an average diameter for the individual micelles of $d = 5.0$ nm.[14,15] However, to explain this discrepancy two facts have to be taken into consideration: (a) Since the freeze drying preparation does not allow to differentiate between individual and assembled micelles it cannot be excluded that multiple superstructures contribute to the histogram in Figure 9d, thus both shifting the average diameter and widening the distribution to larger values. (b) Furthermore, it has been shown that with adsorption to a substrate the cylindrical micellar structures undergo a deformation process toward an ellipsoidal shape which leads to a flattening in height and thus increase of the width of the projection seen in the electron micrographs. Since it is obvious from the results reported so

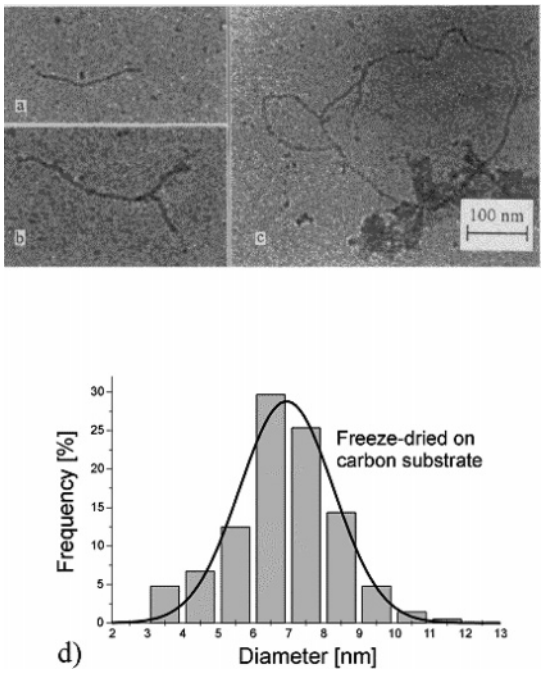

Figure 9. (a−c) TEM micrographs of freeze-dried PPPS-H54 structures deposited on a carbon-coated grid: (a, b) rodlike structures and (c) big loops. (d) Size distribution of the diameters of rodlike structures of PPPSH samples prepared by freeze drying.

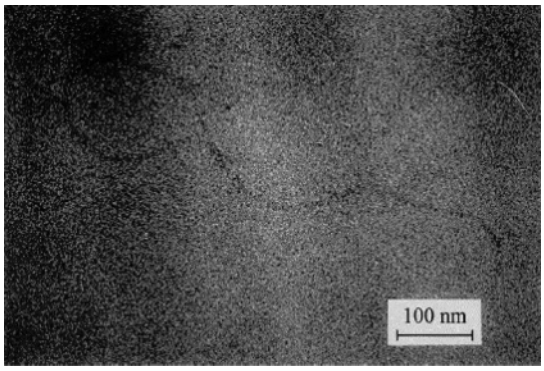

Figure 10. TEM micrograph showing a micellar looplike structure of PPPS-H54 embedded in a thin film matrix of trehalose without any staining agents.

far that interactions of the ionic micelles with substrates and support surface may lead to artifacts in the observation, another strategy was tried.

It has been suggested by Harris[24,25] that aqueous preparations of biological samples could be spread across holey carbon films, when up to 1% of trehalose was added. The sample material is then supported only by the surrounding negative stain and trehalose in solution which dries as a thin amorphous/vitreous film that totally embraces the sample. This procedure was used to prepare PPPS-H samples. It was found that this preparation also works without staining agents by only embedding the sample in a thin film of trehalose. But in this case one has to cope with the extremely small contrast difference between the sample and the surrounding trehalose matrix. Figure 10 shows a TEM micrograph of a PPPS-H54 micellar structure embedded in a thin film of vitreous trehalose. The average diameter of the lasso-shaped structure of a contour length of nearly one micrometer is found to be around 8.0 nm with very little deviation along the trajectory. This micrograph had to be recorded using phase contrast conditions, because of the very small contrast variation between object and matrix. Therefore,

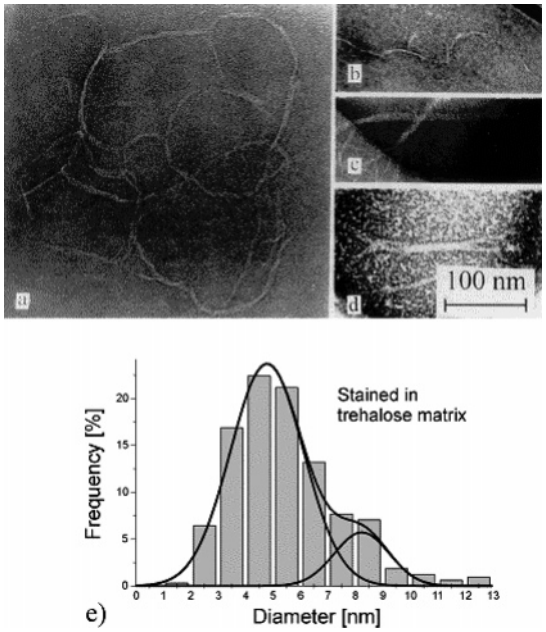

Figure 11. (a−d) TEM micrographs of PPPS-H54 samples negatively stained and embedded in a thin film matrix of trehalose: (a) stained with 5% uranyl acetate at 1% trehalose on a 600 mesh TEM-grid; (b) same as part a but stained with 5% ammonium molybdate and fixed with 0.13% trehalose; (c and d) prepared like sample a but using a holey carbon template. (e) Thickness distribution for rodlike structures prepared by using the stained trehalose film.

the imaged structure appears with a larger diameter, due to the application under focus conditions when recording the micrograph.[34] The implications of the formation of loops which are here seen and reported for the first time will be discussed later.

Because of the poor contrast of the unstained trehalose preparations negative stain was added. The principle of negative staining relates to the imaging of a thinly spread particulate material by surrounding it with a heavy-metal salt in solution and allowing the solution to dry, thereby embedding the material in an amorphous electron-dense layer. Negatively stained samples involving holey templates (holey carbon films or 600 mesh copper grids) have been investigated in this context. The micrographs shown in Figure 11, parts a−d, have been obtained using 2% w/v uranyl acetate with 1% w/v trehalose on a 600 mesh grid (Figure 11a) and on a holey carbon film (Figure 11, parts c and d). Figure 11b shows a PPPS-H54 sample prepared by using 2% w/v ammonium molybdate solution with 1% w/v trehalose on a 600 mesh TEM grid. Again, threadlike objects with different superstructures and complex morphologies can be observed. Figure 11a shows a section of a network of knotted filaments. One can identify the nature of these superstructures being composed of several individual overlong stretches of parallelly assembled micelles. Light scattering studies[10] had shown that PPPS-Na forms clusters and eventually gels at concentrations higher than 0.1 g/L, a concentration, which is typically achieved in the course of the drying process. Thus, this micrograph may serve as a good indication how to picture the nature of these clusters and gels.

Likewise, individual micelles have been detected (Figure 11b, $d \sim 3.6$ nm) but their total amount, compared to the other preparation techniques, was rather low. Similar results, but with a much smaller field of view, have been achieved using holey carbon templates instead of 600 mesh copper grids (Figure 11, parts c and d). In the lower left corner of Figure 11c, the carbon support film is visible, at the upper right one can find the hole which is bridged with the thin trehalose/stain film. The PPPS-H structures are visible as they are embedded in this film and as they are attached to the carbon support. Closer inspection reveals that the degree of branching is higher on the carbon support than within the matrix. Accordingly, the trehalose/stain matrix seems to enhance the self-assembly processes (or the carbon support suppresses them). Figure 11e displays again the histogram of diameters measured for a large number of such objects at different positions along the trajectory. The histogram contains data from both ammonium molybdate and uranyl acetate stained samples in a trehalose thin film matrix. Diameters ranging from 2 nm to approximately 13 nm are covered with the mean value of this distribution located at $d = 5.5$ nm. Again, the histogram may be interpreted in terms of two populations. Fitting the available data by two Gaussians yields mean $d =$ 4.8 and 8.2 nm, respectively. The first one can be interpreted as d of single micelles, matching the scattering data[14,15] quite well. The latter value indicates the existence of "twin"-superstructures composed of two individual micelles.

Recalling the differences in the observed diameters of the micellar structures and correlating them to the different preparation methods, it seems that there is a distinct difference between the data for the stained and the unstained samples. When adding a staining agent the detected diameter for the individual micelle is smaller ($d \sim 5$ nm) than for those preparations without staining ($d \sim 6.8$ nm for the freeze-dried, $d \sim 8$ nm for the pure trehalose matrix). However, it is known from light scattering of dilute solutions[15] that upon addition of salt (e.g., NaCl) the micelles influence in cross section. One may, thus, expect that the same will occur upon the addition of uranyl- and molybdate salt to the dilute solution of PPPS-H. Furthermore, we cannot exclude that the micelles suffer from different interactive forces when they come in contact with the substrate depending on their surface charge which, in turn, is changed by the staining agent.

The existence of lassolike structures and loops in all of the images is an unexpected finding in view of the light scattering result. We emphasize, however, that light scattering is an ensemble average technique, whereas single molecule experiments can probe individual structures. Moreover, the unknown population and form factors of these structures preclude an alternative interpretation of the light scattering intensity distribution $I(q)$, measured over a limited q range. Molar mass, overall length, and linear mass density are reliable measures and hence the rodlike micellar objects dominate. However, these features of lassolike structures and loops deserve closer inspection and an in depth discussion since it gives a clue on the dynamics of the micellar aggregates, their formation, equilibration of their length and nature of their ends.

A histogram of the distribution of the mean diameter of the looplike structures observed in the various preparations is shown in Figure 12. The average diameter of 90 nm is compatible to the estimated persistence length of the micelles of this polyelectrolyte.[14] Seeing such morphology, one is reminded to the case of DNA, where the average diameter of the condensed torroids formed by addition of polyvalent cations is comparable to the DNA persistence length. Acting filaments are stiff and characterized by a rather large persistence length on the order of 10 μm, the diameter of a polycation induced acting ring is in the order of micrometers, much larger than that of DNA torroids, thus reflecting the greater bending stiffness of F-Acting.[35] Impressive morphological similarities of this synthetic polyelectrolyte with biological polymers like circular DNA[36] and also polysaccharides[36] is thus revealed.

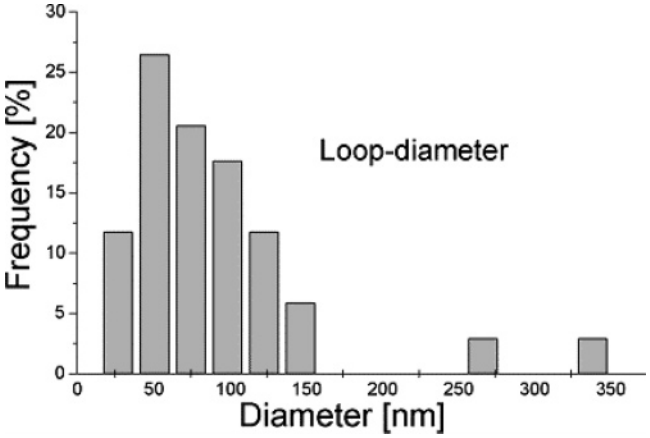

Figure 12. Histogram showing the loop diameter distribution of micellar structures of PPPS-H54 prepared with different methods (staining or freeze drying) and adsorbed on a carbon surface.

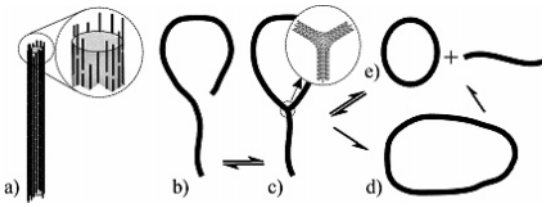

Figure 13. Schematic representation of a possible mechanism for the formation of the closed looplike structures observed.

TEM micrographs of a renaturated polysaccharide schizophyllan[37] showed rodlike structures to coexist with loops and with species involving both circular and linear portions. Some higher molecular weight schizophyllan samples appeared to form twisted or super helical circular species but not all of the macro rings displayed this characteristic. The large rings are thought to be stabilized by the same intrachain interactions that stabilize the parent linear triple helices.

TEM micrographs of open circular DNA molecules[38] after addition of spermine and uranyl salt at various stages in the formation of toroidal compaction revealed (a) extended nets of parallel DNA fibers, (b) the formation of terminal loops by super coiling of the oligomeric circular plasmids, and (c) the formation of a loop by winding around a preformed loop at one end of the circular DNA. The uranyl salt was shown to be responsible for the toroidal compaction of DNA. All these DNA structures show exceptional similarities with the ones of PPPS-H (cf. Figure 7).

Moreover, these results correlate well with that obtained for the complexes formed between plasmid DNA and a PEG−poly(amidoamine) triblock copolymer.[39] The formation of rings was caught by TEM at its initial stages, that is via the bending of a linear structure was captured, implying that is how the rings are formed. This is comparable to the existing theory that toroids are formed from rods.[40,41]

Factors governing and controlling the ring formation need a short discussion here. Formation of a ring involves an energetic penalty because in a cyclic structure of sufficiently small radius of curvature the polymer chain (whether part of a single strand, duplex or triplex domain) will suffer flexural stress.[42] The entropic penalty for ring closure simply reflects the reduction in configurational freedom of the statistical elements of the chain, reducing the number of possible paths of the chain trajectory.[43] As the micelles under consideration here are to be modeled as wormlike objects of very large persistence length this entropic penalty is assumed to be very small. However, there is another aspect specific to ring closure of cylindrical micelles composed of a larger number of individual macromolecules having a distribution of chain length. This argument reflects the situation of chain topology at the ends of the micelles. These must be looked at as surfaces of very high energy since it is unlikely that all chains match with their individual end groups to the end surface of the micelles. These will be rather characterized by a large degree of disorder with regards to the placement of polymer chain ends and dangling segments. Ring closure of the micelles would provide an easy path to relax these constraints in the light that everything points to a liquid-crystalline nematic-type packing of the macromolecules within the micelles.

Parts b and d of Figure 7 show structures of PPPS-H54 that seem to be loops which were formed via the bending of linear structures (which may also have loops at either end). A suggestion of the possible pathway for the formation of a loop in cylindrical micelles is given in Figure 13. Here, the unfavorable situation at the tip of an individual micelle is schematically depicted in Figure 13a. The fringes composed of the constituent chains of the micelle lead to high surface energy. This is comparable to the energetic situation and topology in fibrillar polymer crystals discussed first by Zachmann.[44] The wormlike dynamics of the micelle in dilute solution is associated with a certain probability for the tip to get into contact with its own stem (intramicellar) as depicted in Figure 13b. Since the PPPS-H micelles exhibit a nematic liquid crystalline packing, it is possible to incorporate the tip into a continuous strand via the formation of a disclination ($s = -1/2$) (Figure 13c). Here, the energetic penalty for the formation of a disclination is compensated by the gain of free energy from terminating the unfavorable tip topology. The nature of this kind of disclination is sketched in Figure 13c as a 2D illustration. Once such a loop is formed it can change its morphology further on following two major routes. (a) In order to reduce flexural energy, the loop may grow by moving the disclination in direction to the free end of the micelle which finally will terminate both, the free tip and the disclination, yielding a closed micellar loop (Figure 13d). (b) Due to thermal activation, the loop might break apart, preferentially directly at the disclination and thus yielding either two individual structures, namely a closed loop and a wormlike micelle (Figure 13e) or one individual micelle as depicted in Figure 13b. In thermal equilibrium these processes may proceed in both directions and may involve intermicellar interactions as well. Hence, the great variety of morphologies observed by TEM examination can be produced and explained via these basic processes.

Finally, a critical comparison of similarities and differences in the images obtained by the different techniques provides information to what extend sample preparation affects the observed morphology. The structures revealed by each imaging technique are morphologically largely similar and thus must result from the polymer rather than the sample preparation process as long as effects can be excluded due to changes in concentration which cause aggregation to geld in the case of PPPS-H. Examination of the values obtained for the diameter these rodlike and looplike structures obtained using different techniques or preparation protocols highlight the undesirable effect of adsorption of the sample on the amorphous carbon support in TEM and dehydration of the sample. It is, therefore, difficult if not impossible to retrieve the "true" diameter of the micelles from either of the direct imaging methods. The results do, however, substantiate the model on which the evaluation of scattering data was performed and discussed.

Conclusion

In this paper, we present a detailed analysis of the supramolecular structure formation of a conformationally rigid dodecyl-substituted poly(*p*-phenylene)sulfonate in the free acid form (PPPS-H)—in other words, only hydrated protons serve as counterions in water as the solvent. In very dilute aqueous solutions PPPS-H self-organized into highly anisotropic cylindrical micelles. For several samples of PPPS-H of identical chemical structure and different molar mass $M_{w,p}$ of the constituting polymer, the molar mass, the diameter and the average length of the formed micelles have been determined. The shape of the objects can be described in terms of a weakly bending rod by Koyama's form factor. PPPS-H of $M_{w,p} = 21-58$ kg/mol forms cylindrical micelles of a weight-average length of ~600−1600 nm that is about ~5 times the length of the individual constituent macromolecules. Their cross section contains about ~15 such individual macromolecules aligned along the cylinder axis of the micelle. Thus, the lengthwise aggregation is not controlled by kinetics.

Transmission electron microscopy reveals that the polymer can appear in many different supramolecular forms of aggregates which are composed of cylindrical micelles as the smallest morphological subunit. However, the nature and details of the various forms of aggregation depend largely on the preparation protocol and methods of the samples for TEM inspection. One of the major obstacles consists in difficulties to avoid formation of gels composed of strands of micelles while the solvent is removed from dilute solutions of the micelles in salt-free water. Freeze-drying or even better -embedding of the feeble micellar objects in a vitreous matrix of trehalose helps to preserve the individual micelles. Other artefacts are introduced by contact of the micellar objects with the support, e.g., carbon film for TEM studies. Partial or complete wetting of the support surface by the polyelectrolyte macromolecules deforms the cross-sectional dimensions. Similarly, addition of staining agents causes aggregation phenomena into the direction of clusters or gels of many individual micelles.[15] Nevertheless, the salient features, that is the existence of individual micelles of defined cross-section is well established.

A feature which is clearly established despite differences in detail between the various direct imaging methods is the formation of closed loops and lassolike structures starting from the individual micelles. On the basis of the reasonable assumption on that the packing of the constituent PPPS-H chains within the individual micelles is of nematic and thus fluid character, a mechanism for the formation of closed loops has been suggested. This mechanism allows also for thermal equilibration with regard to the length of the micelles, and it is akin to growth of droplets by collision in oil-in-water emulsions. The driving force for formation of closed loops or lassos is suggested to come from the removal of the entropically unfavorable topology of the macromolecules at the trip of the micelles forming fringes of dangling chains. This process may also lead to reversible cross-links between individual micelles and may contribute to the formation and dynamics of gels of PPPS-H. The branch points would -in the simplest case- involve the microscopic topology of a pinned disclination of strength $-1/2$.

Finally, few theoretical attempts to rationalize the well-defined supramolecular structures have already been reported.[45,46]

Acknowledgment. Financial support from the Max-Planck Society in terms of a postdoctoral fellowship is gratefully acknowledged by C.D. The authors thank Prof. Dr. M. Schmidt from the Department of Physical Chemistry at Johannes Gutenberg-University of Mainz for suggesting us the Koyama form factor as well as A. Larsen and Dr. E. van Ruymbeke from the Department of Materials Science and Technology at University of Crete and F.O.R.T.H. for the assistance in some computations.

References and Notes

(1) Holm, C.; Rehan, M.; Oppermann, W.; Ballauff, M. *Adv. Polym. Sci.* **2004**, *166*, 1.
(2) Barrat, J.-L.; Joanny, J. F. *Adv. Chem. Phys.* **1996**, *94*, 1.
(3) Schmitz, K. S. *Macroions in Solution and Colloidal Suspension*, VCH Publishers: New York, 1993.
(4) Muthukumar, M. *J. Chem. Phys.* **2004**, *120*, 9343.
(5) (a) Ise, N.; Sogami, I. S. *Structure Formation in Solution: Ionic Polymers and Colloidal Particles*, Springer: Heidelberg, Germany, 2005. (b) Noda, I., Kokufuta, E., Ed. *Polyelectrolytes*; Yamady Sci. Foundation: Osaka, Japan, 1999.
(6) Rulkens, R.; Wegner, G.; Enkelmann, V.; Schulze, M. *Ber. Bunsen-Ges. Phys. Chem.* **1996**, *100*, 707.
(7) Bockstaller, M.; Köhler, W.; Wegner, G.; Vlassopoulos, D.; Fytas, G. *Macromolecules* **2000**, *33*, 3951.
(8) Vanhee, S.; Rulkens, R.; Lehmann, U.; Rosenauer, Ch; Schulz, M.; Koehler, W.; Wegner, G. *Macromolecules* **1996**, *29*, 5136.
(9) Rulkens, R.; Wegner, G.; Thurn-Albrecht, T. *Langmuir* **1999**, *15*, 4022.
(10) (a) Bockstaller, M.; Köhler, W.; Wegner, G.; Fytas, G. *Macromolecules* **2001**, *34*, 6353. (b) Bockstaller, M.; Köhler, W.; Wegner, G.; Vlassopoulos, D.; Fytas, G. *Macromolecules* **2001**, *34*, 6359.
(11) Kötz, J. Kosmella, S. Beitz, T. *Prog. Polym. Sci.* **2001**, *26*, 1199.
(12) Bockstaller, M.; Köhler, W.; Wegner, G.; Vlassopoulos, D.; Fytas, G. *Macromolecules* **2000**, *33*, 3951.
(13) Zaroslov, Yu. D.; Gordelily, V. I.; Kuklin, A. I.; Islamov, A. H.; Philippova, O. E.; Khokhlov, A. R.; Wegner, G. *Macromolecules* **2002**, *35*, 4466.
(14) Belack, J. Ph.D. Thesis, Johannes-Gutenberg-Universität, Mainz, Germany, 2000.
(15) Kroeger, A.; Belack, J.; Larsen, A.; Fytas, G. Wegner, G. *Macromolecules* **2006**, *39*, 7098.
(16) Rulkens, R.; Wegner, G.; Enkelmann, V.; Schulze, M. *Ber. Bunsen-Ges. Phys. Chem.* **1996**, *100*, 707.
(17) Belack, J. Ph.D. Thesis, Johannes-Gutenberg-Universität, Mainz, Germany, 2000.
(18) Thurmond, D. *J. Polym. Sci.* **1952**, *8*, 607.
(19) Becker, A.; Köhler, W.; Müller, B. *Ber. Bunsen-Ges. Phys. Chem.* **1995**, *99*, 600.
(20) Kratochvil, P. *Classical Light Scattering from Polymer Solutions*; Elsevier: Amsterdam, 1987.
(21) Brown, W., Ed. *Dynamic Light Scattering*; Clarendon Press: Oxford, U.K., 1993.
(22) (a) Provencher, S. W. *Makromol. Chem.* **1979**, *180*, 201. (b) Provencher, S. W. *Comput. Phys. Commun.* **1982**, *27*, 213 and 229. (c) Stepanek, P. Data Analysis in Dynamic Light Scattering. In *Dynamic Light Scattering*; Brown, W., Ed.; Clarendon Press: Oxford, U.K., 1993.
(23) (a) Patterson, G. D. *Adv. Polym. Sci.* **1983**, *48*, 125. (b) Stevens, J. R. In *Current Topics in Polymer Science*; Ottenbrite, R. N., Ed.; Hauer: München, Germany, 1987. (c) Hagenah, J. V.; Meier, G.; Fytas, G.; Fischer, E. W. *J. Polym. Sci.* **1987**, *19*, 441. (d) Meier, G.; Fytas, G. *Optical Techniques to Characterize Polymer Systems*; Bässler, H., Ed.; Elsevier: Amsterdam, 1989.
(24) (a) Harris, J. R.; Gebauer, W.; Markl, J. *Micron* **1995**, *26*, 25. (b) Harris, J. R. In *Negative Staining and Cryoelectron Microscopy: the thin film techniques*; RMS Handbook No. 35; BIOS Scientific: Oxford, U.K., 1997.
(25) Harris, J. R.; Scheffler, D. *Micron* **2002**, *33*, 461.
(26) (a) Burchard, W. *Ad. Polym. Sci.* **1983**, *48*, 1. (b) Higgins, J.; Benoit, H. *Polymers and Neutron Scattering*; Oxford University Press: Oxford, U.K., 1996.
(27) Schmidt, M. *Macromolecules* **1984**, *17*, 553.
(28) (a) Koyama, R. J. *J. Phys. Soc. Jpn.* **1973**, *34*, 1029. (b) Schmidt, M.; Paradosi, G.; Burchard, W. *Macromol. Chem. Rapid Commun.* **1985**, *6*, 767. (c) Lang, P.; Kajiwara, K.; Burchard, W. *Macromolecules* **1993**, *26*, 3992. (d) Pötschke, D.; Hickl, P.; Ballauf, M.; Astrand, P.-O.; Pedersen, J. S. *Macromol. Theory Simul.* **2000**, *9*, 345.
(29) Fütterer, T.; Hellwig, T.; Findenegg, G. H.; Frahn, J.; Schlüter, A. D. *Macromolecules* **2005**, *38*, 7443 and 7451.
(30) (a) Burchard, W. *Macromolecules* **1978**, *11*, 455. (b) Schmidt, M.; Burchard, W. *Macromolecules* **1978**, *11*, 460.
(31) K. Zero, K.; Pecora, R. Dynamic Depolarized Light Scattering. In *Dynamic Light Scattering*; Pecora, R., Ed.; Plenum Press: New York, 1985.
(32) Yamakawa, H.; Fujii, M. *Macromolecules* **1973**, *3*, 407.

(33) Belack, J.; Wiegand, S.; Janshoff, A. 2006, manuscript in preparation.
(34) Reimer, L. *Transmission Electron Microscopy*; Springer-Verlag: Heidelberg, Germany, Berlin, New York, and Tokyo, 1984; Chapter 6.
(35) Tang, J. X.; Käs, J. A.; Shah, J. V.; Janmey, P. A. *Eur. Biophys. J.* **2001**, *30*, 477.
(36) (a) Stasiak, A. In *Large Ring Molecules*; Semlyen, J. A., Ed.; Wiley: Chichester, U.K., 1996; Chapter 2. (b) Brant, D. A.; McIntire, T. M. In *Large Ring Molecules*; Semlyen, J. A., Ed.; Wiley: Chichester, U.K., 1996; Chapter 4.
(37) Stokke, B. T.; Elgsäter, A.; Brant, D. A.; Kitamura, S. *Macromolecules* **1991**, *24*, 6349.
(38) Böttcher, C.; Endisch, C.; Fuhrhop, J-H.; Catterall, C.; Eaton, M. *J. Am. Chem. Soc.* **1998**, *120*, 12.
(39) Rackstraw, B. J.; Martin, A. L.; Stolnik, S.; Roberts, C. J.; Garnett, M. C.; Davies, M. C.; Tendler, S. J. B. *Langmuir* **2001**, *17*, 3185.
(40) Dunlap, D. D.; Maggi, A.; Soria, M. R.; Monaco, L. *Nucleic Acids Res.* **1997**, *25*, 3095.
(41) Eickbush, T. H.; Moudrianakis, E. N. *Cell* **1978**, *13*, 295.
(42) Barkley, M. D.; Zimm, B. H. *J. Chem. Phys.* **1979**, *70*, 2991.
(43) Jacobson, H.; Stockmayer, W. H. *J. Chem. Phys.* **1950**, *18*, 1600.
(44) Zachmann, H. G. *Pure Appl. Chem.* **1974**, *38*, 79.
(45) (a) Potemkin, I. I.; Khokhlov, A. R. *J. Chem. Phys.* **2004**, *120*, 10848. (b) Potemkin, I. I.; Oskolkov, N. N.; Khokhlov, A. R.; Reineker, P. *Phys. Rev. E* **2005**, *72*, 021804.
(46) (a) Limbach, H. J.; Holm, C.; Kremer, K. *Macromol. Chem. Phys.* **2005**, *206*, 77. (b) Limbach, H. J.; Sayar, M.; Holm, C. *J. Phys.: Condens. Matter* **2004**, *16*, 2135.

MA061966J